Automated three-dimensional image processing for 2-blastomere and 4-blastomere embryo surgical applications

Ze Song* and James K. Mills

Department of Mechanical and Industrial Engineering,
University of Toronto,
Toronto, Ontario M5S3G8, Canada
Email: ze.song@mail.utoronto.ca
Email: mills@mie.utoronto.ca
*Corresponding author

Abstract: The surgical tool and embryo blastomere locations are crucial to perform cell surgery. This paper presents an automated algorithm to compute blastomere centroids and surgical tool coordinate. The algorithm utilises the camera to procure Z-stack images of the workspace. It uses a three-dimensional (3D) canny filter and k-means clustering to segment and compute 3D centroid of each blastomere. For surgical tool tip location, region of interest (ROI) is established via template matching. 2D canny filter is applied on the ROI to produce segmentation results. These results are compiled together to estimate the 3D tool tip location. All computations are conducted on image plane which provide convenience to implement image-based visual servoing (IBVS) control in the future. With the overall obtained computation variations for 2-blastomere (2B) and 4-blastomere (4B) embryo, the proposed algorithm is suitable for blastomere aspiration alike procedures.

Keywords: image segmentation; computer vision; micro robotics; single cell surgery.

Reference to this paper should be made as follows: Song, Z. and Mills, J.K. (2021) 'Automated three-dimensional image processing for 2-blastomere and 4-blastomere embryo surgical applications', *Int. J. Mechatronics and Automation*, Vol. 8, No. 2, pp.92–99.

Biographical notes: Ze Song is a MASc student from the Department of Mechanical Engineering, University of Toronto. He received his Mechanical Engineering Bachelor's degree at University of Waterloo. His current research interests include computer vision, automation and robotic control, biomedical image processing and cell micro-manipulation.

James K. Mills is with Department of Mechanical Engineering, University of Toronto. He received his PhD degrees in Mechanical Engineering both from the University of Toronto. His recent research interests include control of multi-robots, design and control of high speed machines and micro-scale biological task automation. He has published over 400 papers and supervised over 60 masters and PhD students and a number of post-doctoral fellows. He has been an invited Visiting Professor at the Centre for Artificial Intelligence and Robotics in Bangalore, India, Hong Kong University of Science and Technology, Chinese University of Hong Kong and the City University, Hong Kong.

This paper is a revised and expanded version of a paper entitled 'Real time three-dimensional image processing with application to automated cell surgery visual servoing' presented at 2020 IEEE International Conference on Mechatronics and Automation, Beijing, China, 13–16 October 2020.

1 Introduction

Over the last decade, single biological cell surgery has been rapidly developed and expanded into various different biomedical procedures (Song and Mills, 2020). For example, to facilitate in vitro fertilisation, embryo biopsy is performed, in which one or two blastomeres are extracted from the cleaving embryo and used for pre-implantation genetic diagnosis (PGD) (Braude et al., 2002). Chimera cells can be created by injecting embryonic stem cells (ESCs) into early-stage embryos for medical research purposes (Kraus et al., 2010; Yang et al., 2011; Humięcka et al., 2016). Calcium buffer injection into embryos is commonly used to delay the embryo development process (Snow and Nuccitelli, 1993). Chemical intracellular injection is used to generate fate mapping to observe individual blastomere development (Meyer et al., 2010). These single cell surgical processes are currently carried out manually by highly skilled professionals. Due to the micro scale, such manual operations require careful execution

which normally is very time consuming with low success rate and repeatability. To overcome these limitations, substantial efforts to develop fully automated or partially automated approaches are being undertaken which aim to increase the success rate of these complex procedures.

Image processing is essential to achieve automated single cell surgery. For embryo biomedical surgeries, image processing techniques are used to analyse embryo internal structure and its surrounding environment. From these images, location coordinate inputs of the blastomere centroid and surgical tool tip are calculated for the image-based feedback controller to manipulate cells. To demonstrate 3D image processing algorithms proposed in this paper, this paper considers the blastomere centroid as the target location to perform embryo biopsy and cell injection. To facilitates extraction of image coordinates, many image processing techniques have been studied and implemented in embryo cell segmentation, such as watershed (Koyuncu et al., 2012; Schüffler et al., 2015), intensity thresholding, Laplacian-Gaussian filtering (Meijering, 2012), canny edge detector (Al-Hafiz et al., 2018) and active contour (Wu et al., 2015; Song et al., 2017). Despite the successes of these and other approaches, these techniques have their own limitations. Generally, the application of these methods has utilised two-dimensional (2D) images for processing. Early stage embryo with blastomeres presents a 3D complex structure. Although 2D segmentation can produce useable results, the application of 3D segmentation techniques can analyse and give much more reliable and precise input locations for controller to conduct micro scale automation with higher success rate.

Currently, 3D segmentation is heavily reliant on 3D imaging produced by confocal microscopy (Liu et al., 2011). However, due to their high cost, the use of confocal microscopy is seldom reported in research publications, or in laboratories or industrial facilities. Instead, most laboratories and facilities use brightfield microscopy which produces 2D images. Z-stack images are a widely used technique to express a 3D object with 2D image stacks at different vertically spaced focal planes (Wang et al., 2012). 2D segmentation techniques are applied to each image stack and then the information is compiled from all Z-stack images to estimate embryo internal structure locations, edges, etc. An effective 3D image segmentation algorithm which analyses the entire set of Z-stack images as one 3D matrix input still remains a challenge in this field.

With the obtained input locations from image segmentation, visual servoing is then used to effectively control the motion of the automated surgical process. During the operation, the embryo and its internal structure can shift when external forces are applied. Such forces include embryo outer membrane perforation, surgical tool actuation inside the embryo, etc. Thus, the image processing feedback update rate must be high enough to allow compensation for this location variation of all target objects. A human operator can successfully carry out single cell surgery tasks. However, with breaks in work, time for setup, the throughput rate is relatively low. An automated system which runs continuously can achieve higher throughput and success rates due to greater consistency of results than a human operator. Position-based visual servoing (PBVS) has been implemented in cell micro manipulation with many successes (Wang et al., 2007; Mattos et al., 2009; Karimirad et al., 2014). In contrast, image-based visual servoing (IBVS) however has seldom been reported in the cell surgery literature. Unlike PBVS, IBVS does not require calibration of cameras or tool location before experiments. With this approach, computations can be carried out at a higher rate by avoiding coordinate system conversion from the image plane to a Cartesian frame. In order to implement IBVS controller in the future, this proposed image processing algorithm computes all locations in pixel coordinates. So, they can be used later directly for calculations on image plane.

In this paper, a novel 3D image processing algorithm is proposed for automated 2B and 4B embryo surgery visual servoing applications. This paper is organised into six sections. Section 1 reviews existing methods and outlines the research motives. Section 2 introduces the implemented experimental setup. Section 3 describes blastomere segmentation and centroid estimation for both 2B and 4B mouse embryos. Section 4 describes surgical tool segmentation and tip estimation. Section 5 presents and discusses experimental results and Section 6 concludes the proposed image processing algorithm and its future potential.

2 Experimental setup

Figure 1 shows the complete implemented experimental hardware system. Vision feedback is provided by a Qimaging CMOS camera and a Nikon Ti-U brightfield inverted microscope. A –5 hPa vacuum generator connects to a holding micropipette with 90–120 μm outer diameter and 15–20 μm inner diameter. This holding pipette gently holds the targeted embryo on petri dish surface in culture media under the microscope. A partial zona dissection (PZD) micropipette is selected for this experiment to demonstrate embryo surgical processes. It has an inner diameter of 13–15 μm with 30° angled bevelled spike tip. A computer with Intel Core i7 3.6 GHz CPU and 16 GB RAM is used to receive input image date from the camera and execute the proposed image processing algorithm to generate output information.

The camera and all motorised stages can be controlled via MicroManager 1.4 software. A Python open source package called mmcorepy provides a pipeline which allows Python commands to access MicroManager 1.4. Thus, the camera and all stages can be controlled using Python. Figure 2 shows the structure of a sample Z-stack images (Sidhu, 2019). By cooperating between the camera and microscope focus motor, Z-stack images are acquired through capturing images at consecutive evenly spaced plane along Z direction. The focus motor is controlled to rise from a manually selected start position in a constant step size. This step size determines the spacing between

each layer of the Z-stack images. After the focus motor turns for each step size, the camera is controlled to take a snap. A 60-layer Z-stack images can be acquired through repeating these two steps for 60 times. Figure 3 shows a 3D rendering result based on a sample Z-stack images which is acquired using the described method. This is a relatively fast but effective 2D solution of representing a 3D object.

Figure 1 Experimental hardware system (see online version for colours)

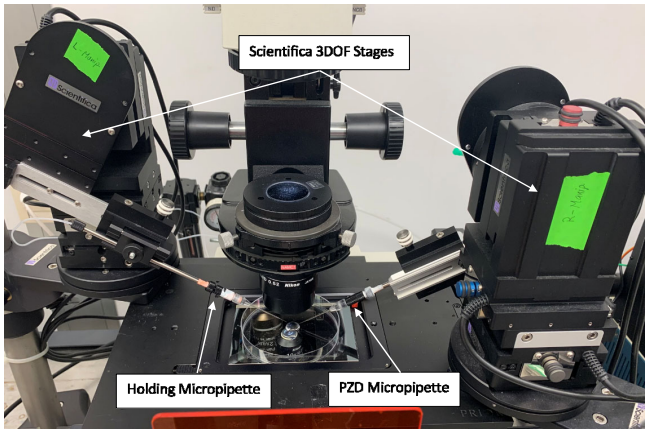

Notes: A prior scientific 3 degree of freedom (DOF) stage moves the holding micropipette under the microscope. The PZD micropipette is held by another Scientifica 3 DOF stage.

Figure 2 2B Z-stack mouse embryo image, (a) images are taken at consecutive evenly spaced image planes along Z direction (b) a 3D blastomere model can be formed by compiling all image slices (see online version for colours)

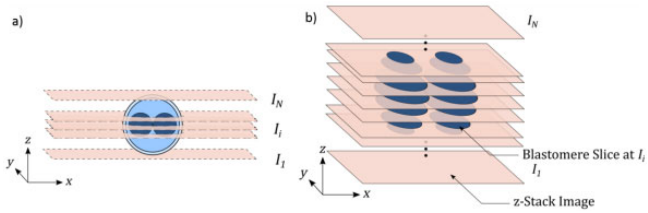

A 10× eyepiece lens and a 20x objective lens from Nikon provide 5.9 µm depth of field. A typical mouse embryo has a size of 100–120 µm. A 120 µm depth of field is captured by 60 stacks of images. A 2 µm spacing is set between every two layers which is less than the depth of field. This ensures the embryo is fully captured by the camera. This CMOS camera has a resolution of 1,920 × 1,080 pixels. To compress the algorithm computation time, a 2 × 2 binning is applied which reduces the resolution by half to 960 × 540 pixels.

Figure 4 demonstrates a sample layer of Z-stack images captured by the described experimental hardware system. Both 2B and 4B mouse embryos are studied for this research. Image processing algorithms are written in Python 3.7 via Jetbrains PyCharm. However, the Python package, mmcorepy, is only available in Python 2.7. A subprocess of calling mmcorepy is created under the main process in Python 3.7 to solve this software version compatibility issue.

Figure 3 3D rendering of a sample Z-stack 2B mouse embryo images (see online version for colours)

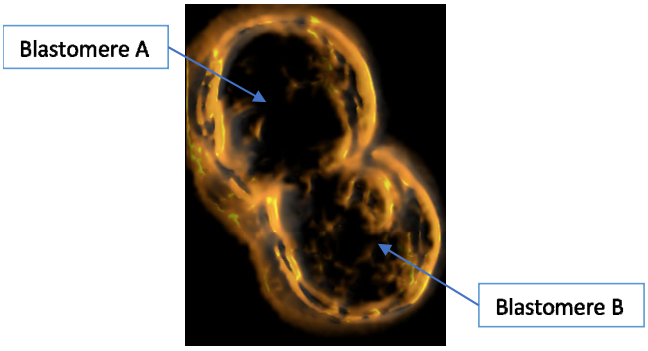

Figure 4 A sample layer of a typical acquired Z-stack images

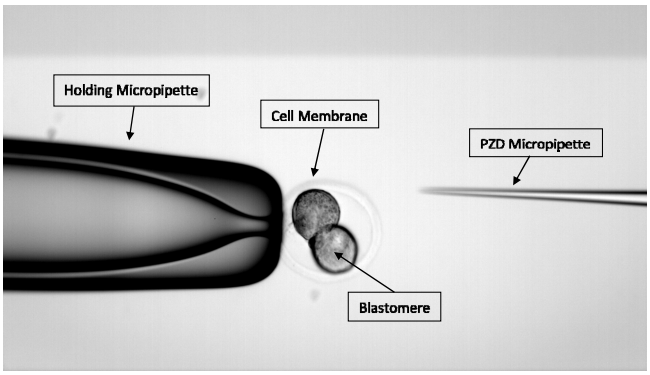

Notes: From left to right, three objects are shown under the microscope: a holding micropipette, a 2B mouse embryo and a PZD micropipette.

3 Blastomere segmentation and centroid estimation

A blastomere image processing algorithm is presented which is compatible for both 2B and 4B mouse embryos. Figure 5 shows a flow diagram of the overall algorithm. To initialise the algorithm, the user needs to first observe the embryo location within the microscope field of view and input the top right corner and bottom left corner of the interested region in pixel coordinates to start the algorithm. These input coordinates are implemented to create a region of interest (ROI) around the embryo on each layer of the Z-stack images. By combining all 60 layers' ROI into one matrix, a 3D volume of interest (VOI) around the embryo is extracted for further processing. Figures 6(a) and 6(d) shows sample 2D ROIs cropped using manual inputs for a 2B and a 4B mouse embryo. By doing so, computation resources are conserved only for interested region. Since the embryo is held by a holding micropipette, the embryo is assumed to stay within the given ROI throughout the entire experiment. Therefore, the manual ROI inputs are only required once to initiate the algorithm. Once the algorithm starts, manual input is no longer required. The algorithm is

capable to complete the task in a fully automated manner with the initial given VOI.

Figure 5 Overall algorithm flow diagram

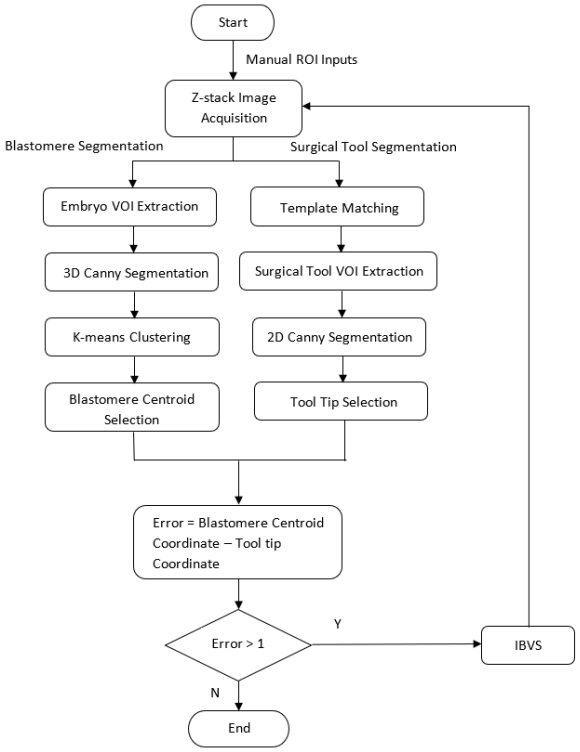

Notes: Manual ROI inputs are used once at the beginning to initialise the algorithm. Then the algorithm is able to keep updating automatically until the error converges.

Second step is to segment the entire VOI as one 3D input matrix utilising a 3D canny edge detector. With the obtained segmentation result, k-means clustering is applied to estimate the 3D centroid location of each blastomere inside the target embryo. The algorithm compares all output centroids and select one which is closest to the right-hand side for surgical operation. All algorithm outputs are calculated in pixel coordinates to provide convenience for future IBVS implementation. Thus, X and Y coordinates in this case represent pixel location in the camera field of view. Z coordinate represents which layer which the centroid is located among the Z-stack images. With 5.9 μm depth of field of the used microscope and 2 μm spacing between adjacent layers of the Z-stack images, 1 pixel along X and Y directions represent 0.322 μm. 1 pixel along Z direction represent 2 μm.

3.1 3D canny edge detector

Canny edge detector provides a moderate method to provide relatively accurate result in a short amount of time. High level techniques include convolutional neural network (CNN), watershed and level sets, take significantly longer time to converge through iterations. On the other hand, Sobel filter and log filter produce noisier data, despite of their faster processing speed.

Three 3D Sobel kernels are first created to convolve within the established VOI. Each kernel is a 3 × 3 filter which calculates pixel intensity gradient along one axial direction as shown in equations (1)–(3). h_x denotes the Sobel kernel along X direction. h_y denotes the Sobel kernel along Y direction. h_z denotes the Sobel kernel along Z direction.

$$h_x(-1,:,:)=\begin{bmatrix}2&2&2\\4&8&4\\2&4&2\end{bmatrix}, h_x(0,:,:)=\begin{bmatrix}0&0&0\\0&0&0\\0&0&0\end{bmatrix}, \quad h_x(1,:,:)=\begin{bmatrix}-2&-4&-2\\-4&-8&-4\\-2&-4&-2\end{bmatrix} \tag{1}$$

$$h_y(:,-1,:)=\begin{bmatrix}2&4&2\\4&8&4\\2&4&2\end{bmatrix}, h_y(:,0,:)=\begin{bmatrix}0&0&0\\0&0&0\\0&0&0\end{bmatrix}, \quad h_y(:,1,:)=\begin{bmatrix}-2&-4&-2\\-4&-8&-4\\-2&-4&-2\end{bmatrix} \tag{2}$$

$$h_z(:,:,-1)=\begin{bmatrix}2&4&2\\4&8&4\\2&4&2\end{bmatrix}, h_z(:,:,0)=\begin{bmatrix}0&0&0\\0&0&0\\0&0&0\end{bmatrix}, \quad h_z(:,1,:)=\begin{bmatrix}-2&-4&-2\\-4&-8&-4\\-2&-4&-2\end{bmatrix} \tag{3}$$

After the gradients along all three coordinate directions are calculated, they are summed using equation (4). d_{sum} denotes the gradient sum of X, Y and Z direction gradients. d_x denotes the X direction gradient. d_y denotes the Y direction gradient. d_z denotes the Z direction gradient.

$$d_{sum}=\sqrt{(d_x)^2+(d_y)^2+(d_z)^2} \tag{4}$$

Figures 6(b) and 6(e) shows the 3D Sobel kernel segmentation results for the processed 2B and 4B mouse embryos in 2D view. From the figures, the algorithm is able to generate fully continuous blastomere contours for further processing.

Hysteresis thresholding uses one high and one low threshold values to enhance and smooth segmented contour. It sets all pixels above the high threshold equals to maximum intensity as start seeding points. For each seeding point, this technique checks its neighbour pixels. Any pixel above the low threshold is set to equal to maximum intensity as well (Mughal et al., 2019). To make the algorithm universally adaptable to different Z-stack images, Otsu thresholding is implemented to calculate the high threshold value based on the intensity distribution for each Z-stack image. This method searches for an optimised threshold that divides pixels into two classes, foreground and background, where inter-class variance is maximised

and intra-class variance is minimised (Otsu, 1979). Low threshold is set to 40% of the calculated Otsu threshold experimentally. Figures 6(c) and 6(f) shows the results after Hysteresis thresholding. Compared with the previous 3D Sobel segmentations, the blastomere contours are much more robust and concise. Customised ratio to compute low threshold from Otsu threshold is suggested if the embryo membrane still appears like in Figure 6(c).

Figure 6 Blatomere image processing in 2D view

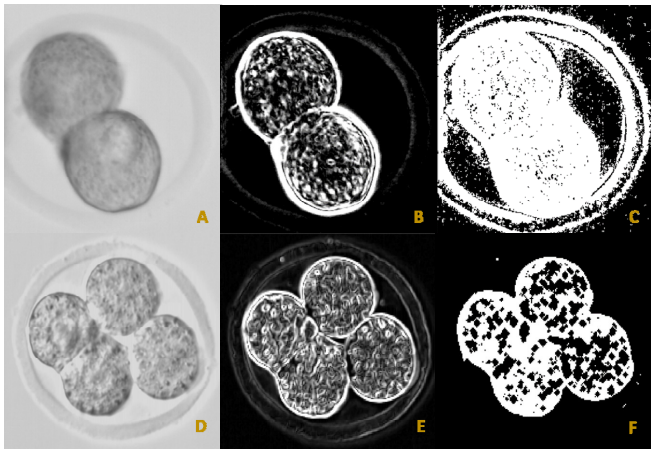

Notes: All images are selected from the sharpest layer from the obtained 3D results. The sharpest layer is defined as the layer with highest intensity distribution standard deviation within the ROI. Figures 6(a), 6(b) and 6(c) shows the image processing at each step for a sample 2B mouse embryo. Figures 6(d), 6(e) and 6(f) shows the same steps for a sample 4B mouse embryo.

3.2 Blastomere 3D centroid estimation

Blastomere centroids are estimated using k-means clustering. This technique is a well-used and simple unsupervised machine learning technique that offers good estimation with high computation efficiency. The objective is to find the placement of k means within the observation set where intra-cluster variance is minimised, and inter-cluster variance is maximised (MacQueen, 1967). The 3D segmentation results are first converted into a 3D data point cloud by removing all black pixels. Only segmented white pixels are taken and converted onto a 3D coordinate system, where X and Y axes represent image pixels and the Z axis represents stacks. The number of means must be manually assigned. Thus, k equals to 2 for 2B embryo and 4 for 4B embryo. Initial means are randomly placed within the 3D point cloud. Through iteration, an optimised k means placement can be found which represents the blastomere centroid locations based on pixel density and distribution.

4 Surgical tool segmentation and tip estimation

It is crucial to know the surgical tool location with fast updating rate, so the assigned task can be precisely performed by designed controller. Normally, micropipettes have symmetrical and regular volumetric shape. Thus, 2D image processing is sufficient to analyse its structure. The ROI for surgical tool is established using template matching, which does not require manual input information. Template matching uses a template image to compute the difference between the template and each section of the test image. The pair with the minimum difference is considered as a match (Brunelli, 2009). Image segmentation uses similar canny edge detection as previously discussed in Section 3. Within the ROI at each layer of Z-stack images, the image is segmented with 2D canny edge detector and complied back into a 3D matrix. The applied 2D Sobel kernel filter is shown in equation (5). Hysteresis thresholding is then implemented on the generated 3D segmentation matrix.

$$h_x = \begin{bmatrix} 1 & 0 & -1 \\ 2 & 0 & -2 \\ 1 & 0 & -2 \end{bmatrix}, h_y = \begin{bmatrix} 1 & 2 & 1 \\ 0 & 0 & 0 \\ -1 & -2 & -1 \end{bmatrix} \quad (5)$$

The tip coordinate is estimated as the furthest point along the segmented contour away from the image edge where the surgical tool appears. Based on implemented experimental setup, it is the furthest point from the image left edge.

5 Experimental results and discussion

The 3D image processing accuracy of both blastomere centroids and the surgical tool tip are difficult to quantitatively verify. Visual inspection is conducted and compared with experimental results. For manual selections, Z coordinates are selected where each blastomere and PZD micropipette visually appear the sharpest among the entire Z-stack images. On the selected sharpest layer, points are manually placed through inspection to represent blastomere centroids and surgical tool tip via ImagJ software. The locations of these manually placed points are then recorded as X and Y coordinates for comparison purpose. Figures 7 and 8 shows the 2B and 4B embryo, respectively, experimental computed and manually selected blastomere centroids and PZD micropipette tip location.

Table 1 shows the comparison of 2B embryo experimental and manual segmentation results. Average pixel differences are 7 and 6 pixels for X and Y direction on the image plane. Average three layer differences are found along Z direction. With 5.9 μm depth of field, each pixel has a dimension of 0.322 × 0.322 μm. Z-stack layers are spaced every 2 μm as discussed in Section 2. Therefore, 2.2 μm and 1.8 μm distance errors are found along X and Y direction respectively. 6 μm distance error is found along Z direction. An average of 6.6 μm direct distance variation between the automated and manual segmented errors is observed. Table 2 shows the comparison of 4B embryo segmentation results. The algorithm has demonstrated very similar accuracy along all three axis directions. 1.3 μm and 2.9 μm distance differences are observed along X and Y direction respectively. 12 μm distance difference has observed along Z direction. A total of 12.4 μm distance error is found

between the calculated and manual selected centroid locations for 4B embryo. High Z direction error in both cases could be caused by relatively large spacing between each image stack. Smaller spacing leads to finer resolution which can be implemented to improve Z direction segmentation accuracy but with a higher computation cost. The image processing accuracy at the current stage is proven suitable to perform tasks for both 2B and 4B mouse embryos, like blastomere aspiration for embryo biopsy. A typical aspiration micropipette has a 30–40 µm inner diameter. For cell injection operations, further improvement is required to implement the proposed algorithm. A typical injection micropipette has a 4–6 µm inner diameter. Ideally, the error must be controlled within 3 µm for this type of applications.

Figure 7 2B embryo auto and manual segmentation result comparisons (see online version for colours)

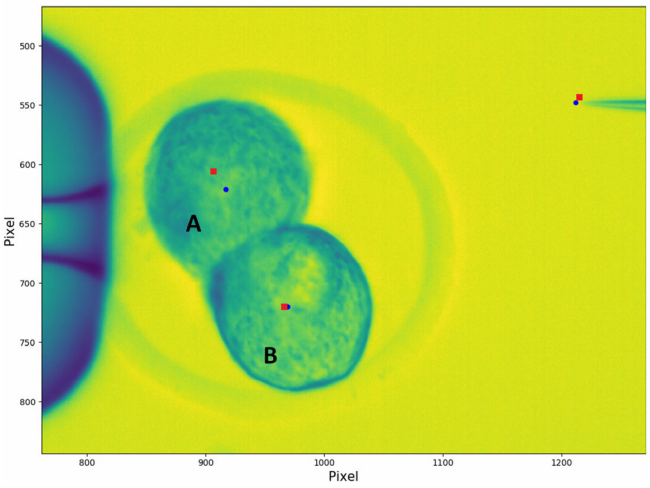

Notes: Red squares shows the computation results of the proposed 3D real time image processing algorithm in 2D views. Blue dots show the manual visual inspection results. High accuracies are achieved on blastomere B and PZD micropipette. The centroid of blastomere A is skewed to the top left direction. Potential cause could be the dense area around the top and left edges of blastomere A.

Table 1 2B embryo experimental and manual result comparison

Object	*Segmentation method*	*X*	*Y*	*Z*
Blastomere A	Auto	606	906	21
	Manual	621	917	18
Blastomere B	Auto	720	966	24
	Manual	720	969	20
PZD micropipette	Auto	543	1,215	25
	Manual	548	1,212	24
Average pixel difference		7	6	3
Average percent error		0.7	0.6	13.6

Table 2 4B embryo experimental and manual result comparison

Object	*Segmentation method*	*X*	*Y*	*Z*
Blastomere A	Auto	632	1,006	21
	Manual	642	1,020	27
Blastomere B	Auto	592	1,120	19
	Manual	590	1,130	27
Blastomere C	Auto	684	1,216	24
	Manual	685	1,205	27
Blastomere D	Auto	714	1,092	22
	Manual	715	1,090	27
Average pixel difference		4	9	6
Average percent error		0.5	0.8	20.4

Figure 8 4B embryo auto and manual segmentation result comparisons (see online version for colours)

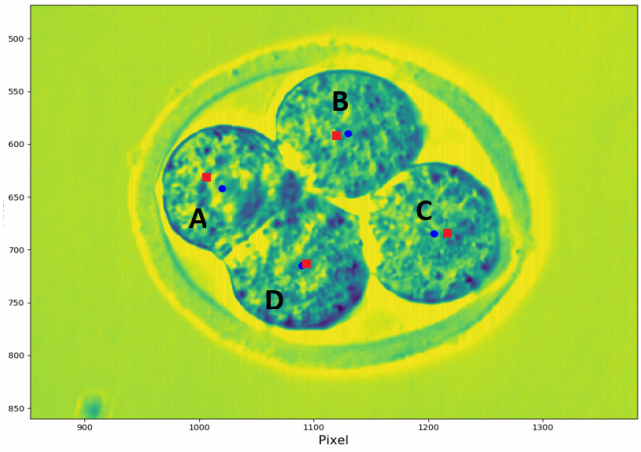

Notes: Red squares shows the computation results of the proposed 3D real time image processing algorithm in 2D view. Blue dots show the manual visual inspection results. High accuracies are achieved on blastomere B, C, D. The centroid of blastomere A is skewed to the top left direction. Potential cause could be the thick embryo emebrane around blatomere A. A customised lower threshold hystersis thresholding should be able to remove the embryo embrane from segmentaion image which will lead to a higher accuracy.

Image processing for 2B and 4B embryo takes around 0.3 s and 0.8 s respectively to extract both the blastomere centroid coordinate and the surgical tool tip coordinate. In this case, both algorithms use 60 stacks of Z-stack images with a resolution of 960 × 540 as inputs. Faster computation time can be achieved by applying 4 × 4 or higher binning setting in the camera to reduce image resolution. However, the processing accuracy drops accordingly. Z-stack images acquisition takes around 5 s to complete. Although the focus motor is set to maximum speed, it still takes longer time than expected to adjust microscope focus 60 times for camera to capture images. Shorter distance between stacks can reduce the image acquisition time with potential loss of

detail at the top and bottom of the embryo. The combined overall algorithm takes around 6 s to complete. Although a human technician can complete the same task as well, but, with constant breaks and work fatigue accumulated during long-hour shifts, the proposed algorithm is still considered to be able to generate faster and more constant throughput.

Figure 9 Test results on different Z-stack embryo images (see online version for colours)

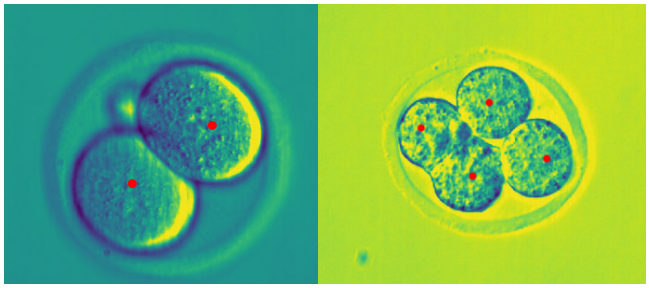

Notes: Red dots represent the estimated blastomere centroids in 2D view.

The algorithm universal adaptability is tested with additional three different Z-stack images for each 2B and 4B embryo. Figure 9 shows the test results of one additional test result for each type of embryo without altering any algorithm parameter. Both trials have demonstrated acceptable centroid estimations, despite different embryo contour, blastomere orientation and development stage.

6 Conclusions

A novel 3D image processing algorithm has been presented in this paper for automated 2B and 4B embryo surgical applications. The proposed algorithm has proven suitable to segment both 2B and 4B embryo and compute 3D centroid for each blastomere within the embryo. All algorithm outputs are calculated on the image plane which can feed into the IBVS controller directly in the future. To initiate the algorithm, manual inputs are first inserted to establish a VOI of the embryo A 3D canny edge detector is applied to segment the acquired Z-stack images within the defined VOI. K-means clustering is utilised to estimate centroid layout based on pixel density and distribution of the segmentation result. Surgical tool location can also be estimated using similar procedures. ROI is established using template matching algorithm. A 2D canny edge detector is used in this case to improve computation efficiency.

Based on the obtained trial results on both 2B and 4B embryo, it is considered that this 3D image processing algorithm has higher accuracy than conventional 2D image processing for cell surgery application. Computation errors of 6.6 μm and 12.4 μm for 2B and 4B embryo segmentation are acceptable to perform blastomere aspiration operations. This image processing algorithm has also demonstrated good universal adaptability to process different Z-stack 2B and 4B mouse embryo images. With finer resolution along Z direction, more precise tasks, like cell injection can be feasible using the presented algorithm.

References

^Al-Hafiz, F., Al-Megren, S. and Kurdi, H. (2018) 'Red blood cell segmentation by thresholding and canny detector', *Procedia Computer Science*, Vol. 141, pp.327–334, DOI: 10.1016/j.procs.2018.10.193.

^Braude, P. et al. (2002) 'Preimplantation genetic diagnosis', *Nature Reviews Genetics*, Vol. 3, pp.941–953, DOI: 10.1038/nrg953.

^Brunelli, R. (2009) 'Template matching techniques in computer vision: theory and practice', DOI: 10.1002/9780470744055.

^Humięcka, M. et al. (2016) 'ESCs injected into the 8-cell stage mouse embryo modify pattern of cleavage and cell lineage specification', *Mechanisms of Development*, Vol. 141, pp.40–50, DOI: 10.1016/j.mod.2016.06.002.

^Karimirad, F. et al. (2014) 'Vision-based robot-assisted biological cell micromanipulation', in *IEEE ROMAN 2014 – 23rd IEEE International Symposium on Robot and Human Interactive Communication: Human-Robot Co-Existence: Adaptive Interfaces and Systems for Daily Life, Therapy, Assistance and Socially Engaging Interactions*, pp.347–352, DOI: 10.1109/ROMAN.2014.6926277.

^Koyuncu, C.F. et al. (2012) 'Smart markers for watershed-based cell segmentation', *PLoS ONE*, Vol. 7, No. 11, DOI: 10.1371/journal.pone.0048664.

^Kraus, P. et al. (2010) 'A more cost effective and rapid high percentage germ-line transmitting chimeric mouse generation procedure via microinjection of 2-cell, 4-cell, and 8-cell embryos with ES and iPS cells', *Genesis*, Vol. 48, No. 6, pp.394–399, DOI: 10.1002/dvg.20627.

^Liu, M. et al. (2011) 'Adaptive cell segmentation and tracking for volumetric confocal microscopy images of a developing plant meristem', *Molecular Plant*, Vol. 4, No. 5, pp.922–931, DOI: 10.1093/mp/ssr071.

^MacQueen, J. (1967) 'Some methods for classification and analysis of multivariate observations', in *Proceedings of the Fifth Berkeley Symposium on Mathematical Statistics and Probability*, pp.281–297.

^Mattos, L.S. et al. (2009) 'Blastocyst microinjection automation', *IEEE Transactions on Information Technology in Biomedicine*, Vol. 13, No. 5, pp.822–831, DOI: 10.1109/TITB.2009.2023664.

^Meijering, E. (2012) 'Cell segmentation: 50 years down the road [life sciences]', *IEEE Signal Processing Magazine*, Vol. 29, No. 5, pp.140–145, DOI: 10.1109/MSP.2012.2204190.

^Meyer, N.P. et al. (2010) 'A comprehensive fate map by intracellular injection of identified blastomeres in the marine polychaete capitella teleta', *EvoDevo*, Vol. 1, No. 1, p.8, DOI: 10.1186/2041-9139-1-8.

^Mughal, B., Muhammad, N. and Sharif, M. (2019) 'Adaptive hysteresis thresholding segmentation technique for localizing the breast masses in the curve stitching domain', *International Journal of Medical Informatics*, Vol. 126, pp.26–34, DOI: 10.1016/j.ijmedinf.2019.02.001.

^Otsu, N. (1979) 'Threshold selection method from gray-level histograms', *IEEE Trans. Syst. Man. Cybern.*, Vol. 9, No. 1, pp.62–66, DOI: 10.1109/TSMC.1979.4310076.

^Schüffler, P.J. et al. (2015) 'Automatic single cell segmentation on highly multiplexed tissue images', *Cytometry Part A*, Vol. 87, No. 10, pp.936–942, DOI: 10.1002/cyto.a.22702.

^Sidhu, S.S. (2019) *Automated Blastomere Segmentation for Visual Servo on Early-stage Embryo*, University of Toronto.

^Snow, P. and Nuccitelli, R. (1993) 'Calcium buffer injections delay cleavage in xenopus laevis blastomeres', *Journal of Cell Biology*, Vol. 122, No. 2, pp.387–394, DOI: 10.1083/jcb.122.2.387.

^Song, T.H. et al. (2017) 'Dual-channel active contour model for megakaryocytic cell segmentation in bone marrow trephine histology images', *IEEE Transactions on Biomedical Engineering*, Vol. 64, No. 12, pp.2913–2923, DOI: 10.1109/TBME.2017.2690863.

^Song, Z. and Mills, J.K. (2020) 'Real time three-dimensional image processing with application to automated cell surgery visual servoing', in *Proceedings of 2020 IEEE International Conference on Mechatronics and Automation*, Beijing, pp.671–676.

^Wang, W. et al. (2007) 'A fully automated robotic system for microinjection of zebrafish embryos', *PLoS ONE*, Vol. 2, No. 9, DOI: 10.1371/journal.pone.0000862.

^Wang, Y. et al. (2012) 'A robust co-localisation measurement utilising Z-stack image intensity similarities for biological studies', *PLoS ONE*, Vol. 7, No. 2, DOI: 10.1371/journal.pone.0030632.

^Wu, P. et al. (2015) 'Active contour-based cell segmentation during freezing and its application in cryopreservation', *IEEE Transactions on Biomedical Engineering*, Vol. 62, No. 1, pp.284–295, DOI: 10.1109/TBME.2014.2350011.

^Yang, H. et al. (2011) 'Mice generated after round spermatid injection into haploid two-cell blastomeres', *Cell Research*, Vol. 21, No. 5, pp.854–857, DOI: 10.1038/cr.2011.45.